MALAYSIAN JOURNAL OF ANALYTICAL SCIENCES

Journal homepage: https://mjas.analis.com.my/

Research Article

Structural, electronic, and optical properties of N/Y-codoped anatase TiO_2: A first-principles investigation

Noor 'Aisyah Johari[1,*], Norjuliyati Hamzah[1], Ahmad Fuzairi Ahmad Faizal[1], Nur Hamizah Mohd Zaki[2,3], Ab Malik Marwan Ali[2,3], Oskar Hasdinor Hassan[3,4], Muhd Zu Azhan Yahya[5], and Mohamad Fariz Mohamad Taib[2,3]

[1]Centre of Foundation Studies, Universiti Teknologi MARA (UiTM), 43800 Dengkil, Selangor, Malaysia
[2]Faculty of Applied Sciences, Universiti Teknologi MARA (UiTM), 40450 Shah Alam, Selangor, Malaysia
[3]Institute of Sciences, Universiti Teknologi MARA (UiTM), 40450 Shah Alam, Selangor, Malaysia
[4]Department of Industrial Ceramic, Faculty of Art and Design, Universiti Teknologi MARA (UiTM), 40450 Shah Alam, Selangor, Malaysia
[5]Faculty of Defence Science and Technology, Universiti Pertahanan Nasional Malaysia (UPNM), 57000 Kuala Lumpur, Malaysia

*Corresponding author: noorai2902@uitm.edu.my

Received: 10 June 2025; Revised: 1 December 2025; Accepted: 1 December 2025; Published: 28 February 2026

Abstract

The influence of N/Y codoping on the structural, electronic, and optical characteristics of anatase TiO_2 is investigated using density function theory. The calculated band gaps are 2.149 eV for pure TiO_2, 1.534 eV for N-doped TiO_2, 2.142 eV for Y-doped TiO_2, and 1.880 eV for N/Y-codoped TiO_2. The slightly lower value of pure TiO_2 compared to the experimental band gap (~3.2 eV) is attributed to the well-known underestimation effect of the GGA-PBEsol functional in DFT calculations. The valence band of pure TiO_2 is mainly composed of O 2*p* states, and the conduction band is mainly composed of Ti 3*d* states. For N-doped TiO_2, the valence band is mainly occupied by N 2*p* states, which are higher than that of the O 2*p* states, which can narrow the band gap. Y doping will introduce 4*d* states, which are involved in the conduction band. As for N/Y codoped, the valence band is mainly occupied by N 2*p* and O 2*p* states, while the conduction band is predominantly occupied by Y 4*d* and Ti 3*d* states. Furthermore, N-doped TiO_2, Y-doped TiO_2, and N/Y-codoped TiO_2 will result in a red-shift of the absorption edge compared with the pure TiO_2 and significantly enhanced in the visible light region.

Keywords: First-principles calculations, density functional theory, TiO_2, N/Y-codoped TiO_2, electronic properties, optical properties

Introduction

Many research articles say that the Honda-Fujishima effect is the first observation of the photocatalytic effect published in Nature in 1972 [1]. A previous work on photocatalytic water splitting using TiO_2 photoelectrodes by Fujishima and Honda marked the dawn of a new era in solar hydrogen harvesting using artificial photosynthesis. In earlier days, TiO_2 was used as a white pigment because it is a low-cost, light-stable, and environmentally friendly material. TiO_2 was mixed with clothing in the 20th century, and it was used for degradation. The photobleaching of dyes by TiO_2 was first reported by Doodeve and Kitchener in 1938 [2]. In addition, the degradation mechanism also explains the UV-absorbed TiO_2, creating the surface-reactive oxygen species known as photosensitizers. Mashio et al. subsequently published on "TiO_2 photocatalyst auto-oxidation" in 1956 [3]. It has been found that H_2O_2 is produced during the photocatalytic reaction. The photocatalytic work was exponentially improved after the discovery of these remarkable results, which were evident from recent scientific publications. Photovoltaic water electrolysis may become more competitive as the cost continues to decrease with technological advancement. However, the considerable use of small band gap semiconducting materials may cause serious life cycle environmental impacts.

Most of the semiconductor photocatalytic materials, such as gallium arsenide (GaAs), lead sulfide (PbS), cadmium sulfide (CdS), zinc oxide (ZnO), iron oxide (Fe_2O_3), tin oxide (SnO_2), and tungsten trioxide (WO_3), have been examined as semiconductor-based photocatalysts [4–7]. Among them, TiO_2 is much more promising as it is stable, non-corrosive, environmentally friendly, abundant, and cost-effective. Rutile, anatase, and brookite are the three

naturally occurring forms of TiO_2. However, because of the complex structure of brookite and difficulties synthesising it in its purest form, more studies are focused on rutile and anatase TiO_2. Anatase TiO_2 is more favourable than rutile and brookite as it has better performance for photocatalytic hydrogen production due to faster charge carrier separation and higher kinetic stability [8, 9]. Unfortunately, the wide band gap of anatase TiO_2 (~3.2 eV) gives a limitation for its light usage in the ultraviolet (UV) region. Therefore, one of the successful methods to reduce the band gap of TiO_2 and thus increase the light harvesting in photocatalytic applications is by doping TiO_2 with non-metal and metal elements.

Doping TiO_2 is an important strategy to modify the band gap and optical response of semiconductor photocatalysts. The main objective of doping is to induce a bathochromic shift as a result decrease in the band gap or introduction of intra-band gap states, which leads to the absorption of more visible light. Doping may lead to photocatalytic systems that exhibit enhanced efficiency [10]. Many studies have been conducted to investigate the doping effect of N-doped TiO_2 theoretically and experimentally [11–16]. Doping by non-metal ions could change the electronic structure and improve the visible light absorption of the photocatalyst by means of narrowing its band gap [17–19]; however, the narrower band gap results in an increased recombination rate of photo-excited carriers, reducing the photocatalytic efficiency. Thus, transition metal element doping can effectively reduce the electron-hole recombination rate. Various research groups have studied TiO_2 doped with many different transition metals [20–24]. Recent studies suggested that transition metal and non-metal codoped in TiO_2 can effectively extend their optical absorption edges from the ultraviolet region to the visible light region and prevent the recombination of electron-hole pairs [25–29].

In this work, the structural, electronic, and optical properties of N-doped TiO_2, Y-doped TiO_2, and N/Y-codoped TiO_2 were studied using the exchange–correlation functional from the GGA method based on the density functional theory (DFT). The doping of N into TiO_2 can reduce its band gap and shift the optical absorption edge toward the visible light region, while the doping of Y into TiO_2 can effectively reduce the electron-hole recombination rate. Both effects are beneficial for improving the performance of the N/Y-codoped TiO_2 photocatalyst. The various manufacturing methods and experimental settings have complex effects on the photocatalytic capabilities of TiO_2; hence, the mechanism of doping is still unclear. Therefore, N-doped TiO_2, Y-doped TiO_2, and N/Y-codoped TiO_2 using DFT need to be studied to clarify the effects on host structural, electronic, and optical properties.

Computational details

Anatase is a metastable mineral form of titanium dioxide (TiO_2). The tetragonal structure of anatase TiO_2 belongs to the spatial group I41/*amd* with lattice parameters $a = b = 3.720$ Å and $c = 9.600$ Å. The non-metal and metal-doped anatase TiO_2 systems using N and Y as dopants were constructed by replacing one Ti atom with a Y atom and one O atom with an N atom in the anatase supercell. In the N/Y-codoped configuration, the N atom substituted an O site, and its adjacent Ti atom was replaced by a Y atom, as shown in Fig. 1. This nearest-neighbor substitution model was selected because it has been reported to be one of the most energetically favorable and structurally stable configurations for N-metal codoped TiO_2 systems. Such close dopant proximity facilitates effective charge transfer and orbital hybridization between N 2*p* and Y 4*d* states, which enhances visible-light absorption. Additionally, the 1:1 substitution ratio minimizes lattice distortion while maintaining computational tractability, consistent with previous DFT codoping studies [30]–[32]. Therefore, this configuration was adopted as a representative and physically meaningful model for evaluating the electronic and optical properties of N/Y-codoped TiO_2.

The first-principles calculations in this work were performed from DFT as implemented in the Cambridge Serial Total Energy Package (CASTEP) computer code. The structural, electronic, and optical properties of N-doped TiO_2, Y-doped TiO_2, and N/Y-codoped anatase TiO_2 were calculated using the best exchange correlation functional, which is from the generalized gradient approximation in the Perdew-Burke-Ernzerhof for solids (GGA-PBEsol) [33]. The cut-off energy of 380 eV was required for N-doped TiO_2, Y-doped TiO_2, and N/Y-codoped anatase TiO_2, while the *k*-point sampling of 4×4×2, 4×4×2, and 3×3×2 was set in Monkhorst-Pack grid for the N-doped TiO_2, Y-doped TiO_2, and N/Y-codoped TiO_2, respectively, which is within the convergence value as verified from the convergence test. Pseudo atomic calculation were $2s^2\ 2p^4$ for O, $3s^2\ 3p^6\ 3d^2\ 4s^2$ for Ti, $2s^2\ 2p^3$ for N and $3s^2\ 3p^6\ 3d^3\ 4s^2\ 4d^1$ for Y. The geometrical optimization was set at 5.0×10^{-6} eV/atom for total energy, 0.01 eV/Å for maximum force, 0.02 GPa for maximum stress, and 5.0×10^{-4} Å for maximum displacement.

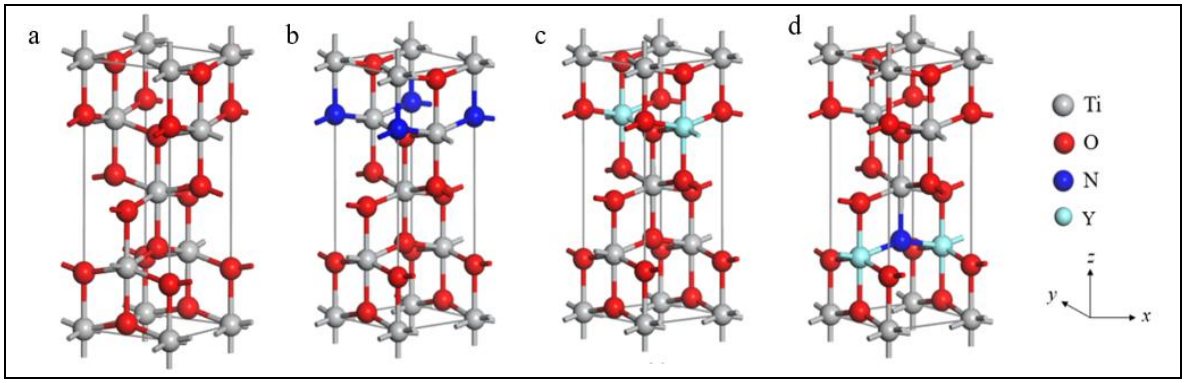

Figure 1. Crystal structures of (a) pure TiO_2; (b) N-doped TiO_2; (c) Y-doped TiO_2; (d) N/Y-codoped TiO_2

Results and Discussion

Structural parameters

The optimized lattice parameters of pure TiO_2, N-doped TiO_2, Y-doped TiO_2, and N/Y-codoped TiO_2 are all listed in **Table 1**. The lattice constants of pure TiO_2 are consistent with those in previous experimental work [34]. This result implies that our calculating methods are acceptable and that the calculated outcomes are reliable.

The optimized cell characteristics for pure TiO_2 and TiO_2 that has been doped with N and Y are compared to examine the changes in geometrical structure brought on by the non-metal and metal dopants. It is found that the lattice parameters of N-doped TiO_2 were overestimated by 2.66% and 1.37% for *a* and *b* parameters, respectively. While lattice parameters of Y-doped TiO_2 were overestimated by 4.03% ($a = b$ parameters) over pure TiO_2. For the *c* parameter, the underestimation of N-doped TiO_2 compared to pure TiO_2 is by 0.27% and for Y-doped TiO_2, the overestimation is by 12.01% compared to pure TiO_2. Compared with the lattice constant ratio (*c*/*a*), the underestimation and overestimation of N-doped TiO_2 and Y-doped TiO_2 are by 2.87% and 10.85% over pure TiO_2. For the volume, the N-doped TiO_2 and Y-doped TiO_2 expand their volume by 3.75% and 21.21%, respectively. For N/Y-codoped TiO_2, it is found that lattice parameters (*a*, *b,* and *c*), lattice constant ratio (*c*/*a*), and volume (V) of the codoping are larger than pure TiO_2. N/Y-codoped TiO_2 was overestimated by 2.55%, 3.36% and 15.35% for *a*, *b,* and *c*, respectively, over pure TiO_2. Compared with the lattice constant ratio (*c*/*a*) of pure TiO_2, the overestimation of N/Y-codoped TiO_2 is 12.48%. For the volume of N/Y-codoped TiO_2, their unit cell volume expands by 22.23%. The increased cell volume of TiO_2 suggests a larger surface area and higher dye-loading capability. This is because the atomic radius of Y (2.12 Å) is larger than Ti (1.76 Å). This optimized TiO_2 structure was used for further calculations to gain a deeper theoretical understanding of its properties.

The average bond length in pure TiO_2, N-doped TiO_2, Y-doped TiO_2, and N/Y-codoped TiO_2 for Ti-O, O-O, N-Ti, V-O, and Y-O are listed in Table 2. In N-doped TiO_2, the Ti-N (1.967 Å) bond lengths are closely similar to Ti-O (1.959 Å) in pure TiO_2 [35]. However, in Y-doped TiO_2, the Y-O (2.511 Å) is longer than Ti-O (1.961 Å) by +0.10%, suggesting that the Y-O bond has weaker covalency than the Ti-O bond. Generally, O-O bond lengths are longer compared to Ti-O, N-Ti, and V-O. The Ti-O bond lengths slightly elongated after the N/Y-codoped TiO_2, as compared to the Ti-O bond lengths before codoping. However, the Y-O is longer than Ti-O and O-O bond lengths. The Y-O bond (2.662 Å) is longer than the Ti-O bond (1.959 Å) by approximately 0.51% in N/Y-codoped TiO_2. It should be noted that the longer bond length leads to a weaker bond strength. Generally, the increase of bond length between cation and anion may decrease the coupling constant and consequently decrease the band gap according to spectroscopic analysis of a set of tetrahedrally coordinated semiconductors [36].

Band structures

The incorporation of N and Y atoms in anatase TiO_2 not only influences the crystal structures but also affects its electronic properties. The band structure of pure TiO_2 [37] was calculated using the first-principles method and is shown in **Figure 2(a)**. The theoretical band gap of anatase TiO_2 calculated using the GGA-PBEsol functional is 2.149 eV, which is lower than the experimental value of approximately 3.2 eV, which is in agreement with previous DFT studies [38–40]. This underestimation is a well-known limitation of conventional GGA-based DFT methods, as they typically neglect the quasiparticle self-energy correction. Despite this, the relative differences between the doped and codoped systems remain valid for understanding the qualitative effects of N and Y incorporation on the electronic structure. The band structures of N-doped TiO_2, Y-doped TiO_2, and N/Y-codoped anatase TiO_2 along the high symmetry directions of the Brillouin zone (BZ) at G(0,0,0)-F(0,0.5,0)-Q(0,0.5,0.5)-Z(0,0,0.5)-G(0,0,0) are shown in **Figure 2(b)-2(d)**.

Table 1. Lattice constants (*a*, *b*, *c*) and volumes (V) of pure TiO_2, N-doped TiO_2, Y-doped TiO_2 and N/Y-codoped TiO_2 by geometry optimization

	Present works				Experimental [34]
	Pure TiO_2	**N-doped TiO_2**	**Y-doped TiO_2**	**N/Y-codoped TiO_2**	**Pure TiO_2**
a (Å)	3.720	3.819 (+2.66%)	3.870 (+4.03%)	3.815 (+2.55%)	3.787
b (Å)	3.720	3.771 (+1.37%)	3.870 (+4.03%)	3.845 (+3.36%)	3.787
c (Å)	9.600	9.574 (-0.27%)	10.753 (+12.01%)	11.074 (+15.35%)	9.514
c/a (Å)	2.581	2.507 (-2.87%)	2.779 (+10.85)	2.903 (+12.48%)	2.512
V ($Å^3$)	132.88	137.86 (+3.75%)	161.07 (+21.21%)	162.42 (+22.23%)	136.44

(+) overestimate; (-) underestimate compared to pure TiO_2

Table 2. Average bond length of doped TiO_2 after geometry optimization

	Pure TiO_2	**N-doped TiO_2**	**Y-doped TiO_2**	**N/Y-codoped TiO_2**
Ti-O (Å)	1.959	1.970 (+0.56%)	1.961 (+0.10%)	1.969 (+0.51%)
O-O (Å)	2.626	2.637 (+0.42%)	2.775 (+5.67%)	2.769 (+5.45%)
N-Ti (Å)	–	1.967	–	1.926
Y-O (Å)	–	–	2.511	2.662

(+) overestimate compared to pure TiO_2

When the non-metal and metal elements are doped in TiO_2, the energy gaps are reduced. For pure anatase TiO_2, the energy band gap is 2.149 eV, while the N-doped TiO_2 and Y-doped anatase TiO_2 show a reduced band gap to 1.534 eV and 2.142 eV, respectively. The N doping causes a slight decrease in the band gap to 1.534 eV in connection with the formation of localized N 2*p* states just above the valence band maximum (VBM) of TiO_2, which can be seen in the density of states (DOS). A decrease in conduction band minimum (CBM) and VBM causes the band gap to widen due to intense nitrogen doping is similar to that described by Liu and co-workers [41]. For Y-doped TiO_2, the CBM moves slightly downward and reduces the band gap by 0.33% compared to pure TiO_2. In addition, the Fermi level moves into the VB and shows the property of a p-type semiconductor. The reduction of energy gaps from the TiO_2 codoping is due to the lowering of the CB. The N/Y-codoped anatase TiO_2 shows a reduced band gap to 1.880 eV. The slight decrease in bandgap values for the rare earth doped could be attributed to size quantization or charge carrier spatial confinement. This is due to the fact that the electron-hole pairs are now considerably closer together, and the Coulombic interaction between them can no longer be ignored, resulting in a larger overall kinetic energy [42].

Density of states

The partial density of states (PDOS) and total density of states (DOS) of N-doped TiO_2, Y-doped TiO_2, and N/Y-codoped TiO_2 are given in **Figure 3** to explore the electronic structures. It is well known that the conduction band of TiO_2 is composed of Ti 3*d* orbital, and the valence band is composed of O 2*p* orbital and in agreement with previous work by other researchers [43]. For the N-doped TiO_2, the orbital hybridization of Ti 3*d*, O 2*p,* and N 2*p* forms the valence band of N-doped TiO_2. After N doping, it is very clear that the empty band appeared in the middle of the forbidden band of TiO_2. The N 2*p* orbital lies near the CBM of TiO_2, which decreases the band gap of TiO_2 and improves the photocatalytic activity.

From the DOS of Y-doped TiO_2, it can be seen that *d* states mostly contribute to the conduction zone, while *p* states contribute mainly to the valence zone. The obtained results are also in agreement with what has been established for Y atoms, and that is the fact that their presence in the structure narrows the band gap, which is of particular importance for photocatalysis [44, 45]. In the case of the N/Y-codoped TiO_2, the Y 4*d* state dominates the conduction band, which is located close to the bottom of the conduction band, while the N 2*p* state dominates the valence band, which is located close to the top of the valence band. From the DOS of N/Y-codoped TiO_2, it can be concluded that the absorption edge transition occurs between N 2*p* and Y 4*d* states.

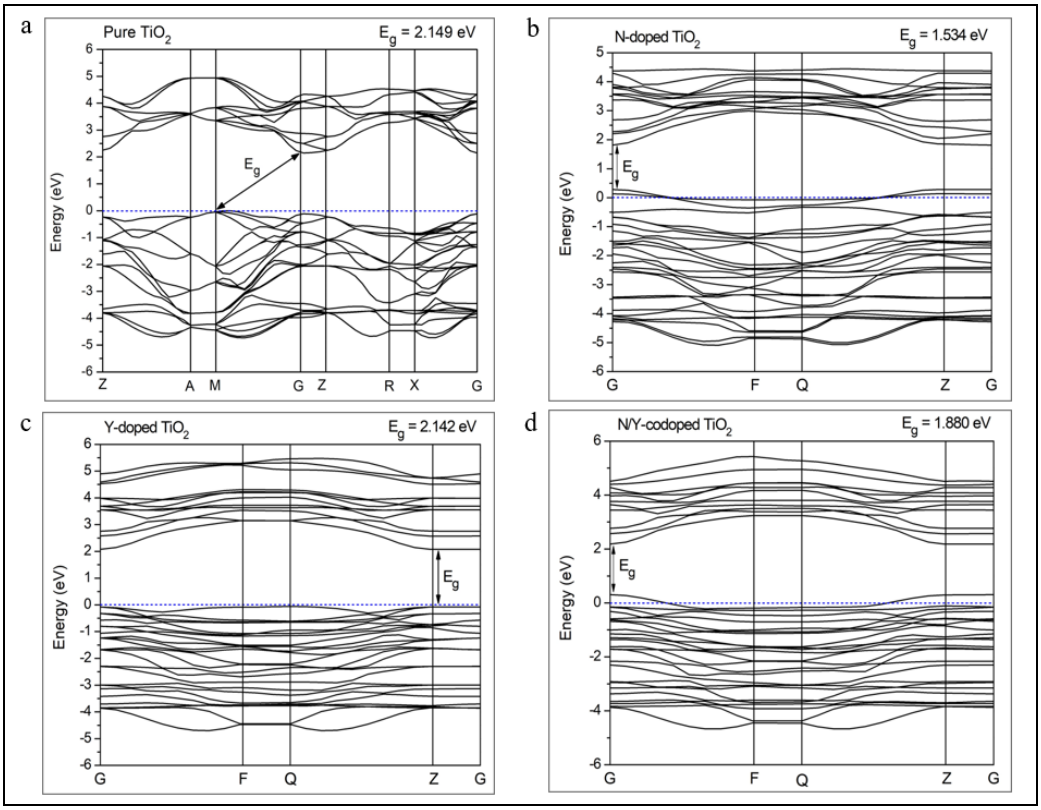

Figure 2. The band structures of (a) pure TiO_2; (b) N-doped TiO_2; (c) Y-doped TiO_2; (d) N/Y-codoped TiO_2. The Fermi energy is set to zero as indicated by the blue dashed line. The calculated values are smaller than experimental results due to the well-known underestimation of band gaps by the GGA-PBEsol functional

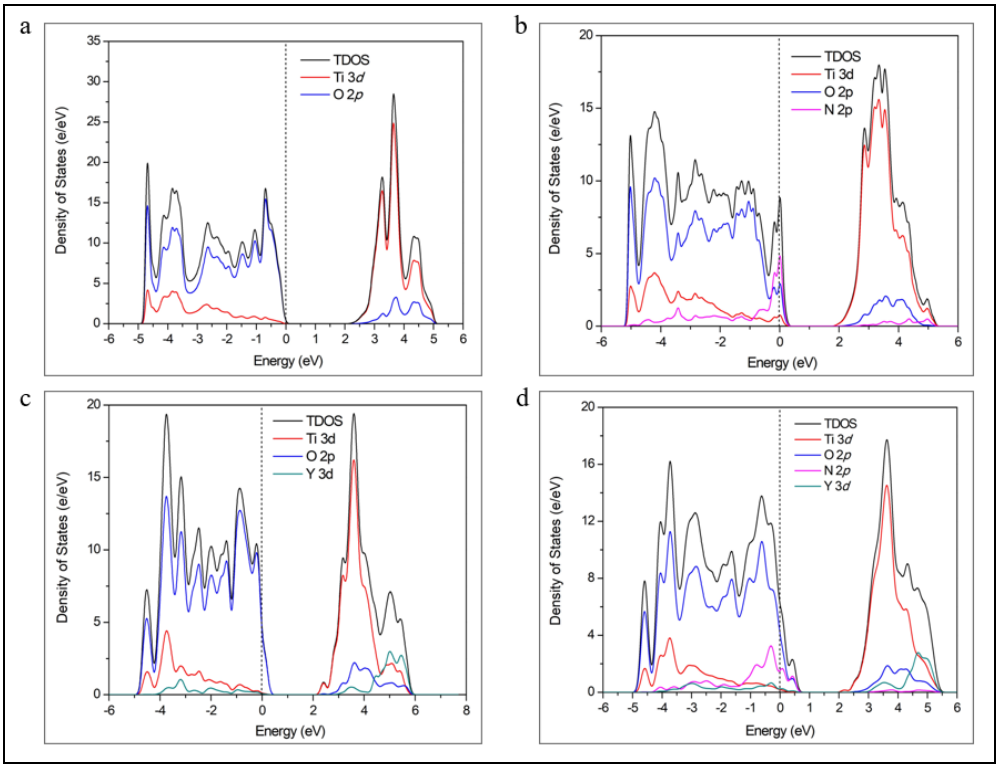

Figure 3. The TDOS and corresponding PDOS of (a) pure TiO_2, (b) N-doped TiO_2, (c) Y-doped TiO_2, and (d) N/Y-codoped TiO_2. The Fermi level is indicated by the black dashed line

Absorption spectra

The absorption coefficients of pure TiO_2, N-doped TiO_2, Y-doped TiO_2, and N/Y-codoped TiO_2 against photon energy and wavelength are displayed in **Figure 4**. The pure TiO_2 exhibits an absorption edge at approximately 2.149 eV (~577 nm), consistent with its ability to primarily absorb UV light. After doping, a clear red-shift in the absorption edge is observed. The absorption onsets shift to ~1.534 eV (~809 nm) for N-doped TiO_2, ~2.142 eV (~579 nm) for Y-doped TiO_2, and ~1.880 eV (~660 nm) for N/Y-codoped TiO_2. This behavior corresponds directly to the calculated band gap values and confirms that doping introduces impurity states that narrow the band gap. Among all systems, the N/Y-codoped TiO_2 exhibits the greatest visible-light absorption enhancement, indicating a synergistic effect where N contributes to valence band elevation while Y influences conduction band states, thereby facilitating improved charge carrier excitation under visible illumination. In conclusion, the electrons in the valence band can be excited to the conduction band by absorption of the visible light, and non-metal and metal doping are ideal to effectively utilize solar energy in the visible light region.

For N-doped TiO_2, the photo-excited carrier will be trapped by the N 2*p* state and then transferred into the conduction band. As shown in **Figure 4 (b)**, the Y-doped TiO_2 system does not show good absorption activity in the visible light region. For the N/Y-codoped TiO_2 system, the transition energy becomes smaller due to the split of the impure state, rendering a more obvious red-shift. Thus, the photocatalytic efficiency is enhanced by suppressing the recombination of electron-hole pairs. Compared with the N-doped TiO_2 and Y-doped TiO_2, the N/Y-codoped TiO_2 is expected to be a more active photocatalyst.

Conclusion

In this study, the structural, electronic, and optical properties of N-doped, Y-doped, and N/Y-codoped anatase TiO_2 were investigated using first-principles calculations within the GGA-PBEsol framework. The results indicate that N doping mainly contributes to the upward shift of the valence band through the introduction of N 2*p* states, while Y doping modifies the conduction band through Y 4*d* states. When codoped, these effects act synergistically, resulting in a more pronounced reduction in the band gap (1.880 eV) compared to single-doped systems and promoting an enhanced red-shift in the optical absorption edge toward the visible-light region. This demonstrates that N/Y codoping is a promising strategy for improving visible-light-driven photocatalytic activity of TiO_2.

However, the present work is limited to bulk electronic structure calculations and does not explicitly consider surface states, charge recombination dynamics, or adsorption/reactive intermediates, which are critical to actual photocatalytic performance. Therefore, future studies should include experimental synthesis and photocatalytic testing, as well as surface reactivity and carrier transport analyses, to verify and further optimize the functional role of N/Y codoping. These additional investigations may help establish a stronger correlation between theoretical predictions and real-world photocatalytic applications.

Acknowledgements

The authors would like to thank the Institute of Science (IOS), Universiti Teknologi MARA (UiTM), and the Ministry of Higher Education Malaysia (MOHE) for the facilities and financial support provided under the research grant UiTM.800-3/1 DDF.88 (001/2025).

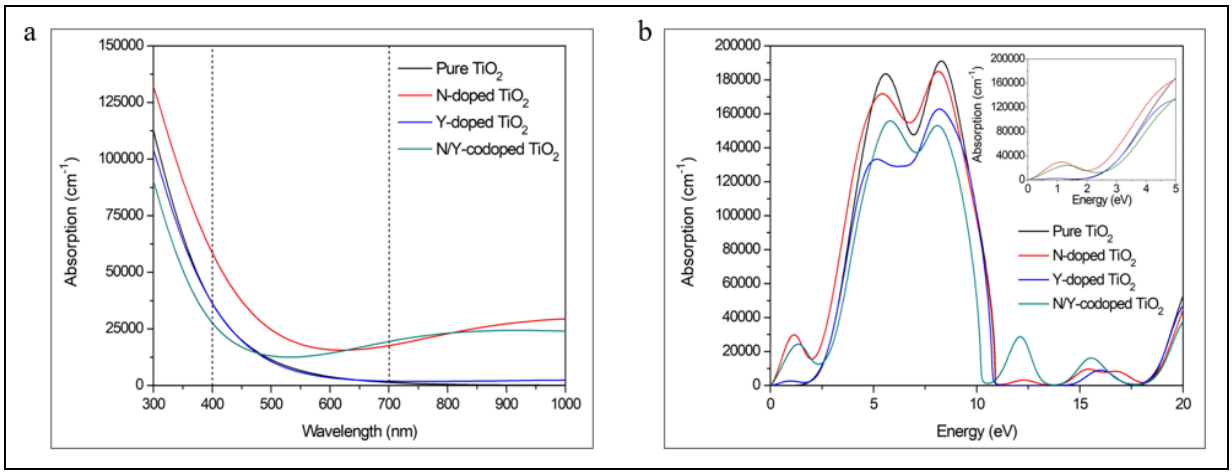

Figure 4. The optical absorption spectra of pure TiO_2, N-doped TiO_2, Y-doped TiO_2, and N/Y-codoped TiO_2 against (a) wavelength (nm) and (b) energy (eV)

References

1. Fujishima, K. and Honda, A. (1972). Electrochemical Photolysis of Water at a Semiconductor Electrode. *Nature*, 238: 37–38.
2. Goodeve, C. F. and Kitchener, J. A. (1938). The Mechanism of Photosensitisation by Solids. *Transactions of Faraday Society*, 34: 902–908.
3. Hashimoto, K., Irie, H. and Fujishima, A. (2005). TiO_2 photocatalysis: A historical overview and future prospects. *Japanese Journal of Applied Physics,* 44(12): 8269–8285.
4. Vafaee, M. and Ghamsari, M. S. (2007) Preparation and characterization of ZnO nanoparticles by a novel sol-gel route. *Materials Letters*, 61: 3265–3268.
5. Sivula, K., Formal, F. L. and Grätzel, M. (2009). WO_3-Fe_2O_3 photoanodes for water splitting: A host scaffold, guest absorber approach. *Chemistry of Materials*, 21(13): 2862–2867.
6. Kohtani, S., Yoshioka, E. and Miyabe, H. (2012). Photocatalytic Hydrogenation on Semiconductor Particles. *Hydrogenation*, 291–308.
7. Huang, S., Luo, W. and Zou, Z. (2013). Band positions and photoelectrochemical properties of Cu_2ZnSnS_4 thin films by the ultrasonic spray pyrolysis method. *Journal of Physics D: Applied Physics*, 46(23): 235108–235114.
8. Xu, M., Gao, Y., Moreno, E. M., Kunst, M., Muhler, M., Wang, Y., Idriss, H. and Wöll, C. (2011). Photocatalytic activity of bulk TiO_2 anatase and rutile single crystals using infrared absorption spectroscopy. *Physical Review Letters*, 106(13): 138302–138305.
9. Mu, R., Zhao, Z. J., Dohnálek, Z. and Gong, J. (2017). Structural motifs of water on metal oxide surfaces. *Chemical Society Reviews*, 46(7): 1785–1806.
10. Carp, O., Huisman, C. L. and Reller, A. (2004). Photoinduced reactivity of titanium dioxide. *Progress in Solid State Chemistry*, 32(1–2): 33–177.
11. Bouzourâa, M. B., Naciri, A. E., Battie, Y., Dalmasso, S., Diliberto, S., Bouché, A. and Chaoui, N. (2022). Correlation between optical and structural properties of nitrogen doped anatase TiO_2 thin films. *Optical Materials*, 133: 112919.
12. Hu, Z., Xu, T., Liu, P. and Oeser, M. (2021). Microstructures and optical performances of nitrogen-vanadium co-doped TiO_2 with enhanced purification efficiency to vehicle exhaust. *Environmental Research*, 193: 110560.
13. Sun, Z., Pichugin, V. F., Evdokimov, K. E., Konishchev, M. E., Syrtanov, M.S., Kudiiarov, V. N., Li, K. and Tverdokhlebov, S. I. (2020) Effect of nitrogen-doping and post annealing on wettability and band gap energy of TiO_2 thin film. *Applied Surface Science*, 500: 144048.
14. Wu, H. C., Lin, S. W. and Wu, J. S. (2012). Effects of nitrogen concentration on N-doped anatase TiO_2: Density functional theory and Hubbard U analysis. *Journal of Alloys and Compounds*, 522: 46–50.
15. Xu, T., Wang, M. and Wang, T. (2019). Effects of N Doping on the Microstructures and Optical Properties of TiO_2. *Journal Wuhan University of Technology, Materials Science Edition*, 34(1): 55–63.
16. Mathis, J. E., Lieffers, J. J., Mitra, C., Reboredo, F. A., Bi, Z., Bridges, C. A., Kidder, M. K. and Paranthaman, M. P. (2016). Increased photocatalytic activity of TiO_2 mesoporous microspheres from codoping with transition metals and nitrogen. *Ceramics International*, 42(2): 3556–3562.
17. Huang, H. C., Yang, C. L., Wang, M. S. and Ma, X. G. (2017). Enhanced photocatalytic performance of anatase TiO_2 substitutionally co-doped with La and N. *Solar Energy Materials and Solar Cells*, 170: 233–238.
18. Valentin, C. D. and Pacchioni, G. (2013). Trends in non-metal doping of anatase TiO_2: B, C, N and F. *Catalysis Today*, 206: 12–18.
19. Zhou, S. W., Peng, P., Liu, J., Tang, Y. H., Meng, B. and Peng, Y. X. (2016). Investigation on the electronic structures and optical performances of Si-S codoped anatase TiO_2 by first-principles calculation. *Physics Letters, Section A: General, Atomic and Solid State Physics*, 380(16): 1462–1468.
20. Pandey, S., Shukla, A. and Tripathi, A. (2022). Effect of pressure on electrical and optical properties of metal doped TiO_2. *Optical Materials*, 133: 112875
21. Ouali, K., Assali, A., Benaissa, S., Benharrat, L. and Berrah, S. (2023). Electronic structure and optical properties of tin (IV) doped transparent perovskite crystal $BaTiO_3$ for efficient visible optoelectronic devices and solar cells. *Materials Today Communications*, 35: 106035.
22. Ishikawa, T., Sahara, R., Ohno, K., Ueda, K. and Narushima, T. (2023). Electronic structure analysis of light-element-doped anatase TiO_2 using all-electron GW approach. *Computational Materials Science*, 220: 112059.
23. Islam, M. N., Podder, J., Hossain, K. S. and Sagadevan, S. (2020). Band gap tuning of p-type Al-doped TiO_2 thin films for gas sensing applications. *Thin Solid Films*, 714: 138382.
24. Cui, Y., Wang, Q., Ren, J., Liu, B., Yang, G. and Gao, Y. (2019). Geometric and electronic properties of rutile TiO_2 with vanadium implantation: A first-principles calculation. *Nuclear Instruments and Methods in Physics Research, Section B: Beam Interactions with Materials and Atoms*, 455: 35–38.
25. Youssef, A. M., Yakout, S. M. and Mousa, S. M. (2023). High relative permittivity and excellent dye photo-elimination: Pure and (Zr^{4+}, Y^{3+}, Sb^{5+}) multi-doped anatase TiO_2 structure. *Optical*

Materials, 135: 113261.
26. Ikram, M., Rashid, M., Haider, A., Naz, S., Haider, J., Raza, A., Ansar, M. T., Uddin, M. K., Ali, N. M., Ahmed, S. S., Imran, M., Dilpazir, S., Khan, Q. and Maqbool, M. (2021). A review of photocatalytic characterization, and environmental cleaning, of metal oxide nanostructured materials. *Sustainable Materials and Technologies*, 30: e00343.
27. Yang, L., Luo, X., Yang, F., Liu, C., Zhang, L. and Tang, J. (2020). Electronic structure and optical properties of C-Pt codoped anatase TiO_2 by first principles. *Optik*, 223: 165588.
28. Phattalung, S. N., Limpijumnong, S. and Yu, J. (2017). Passivated co-doping approach to bandgap narrowing of titanium dioxide with enhanced photocatalytic activity. *Applied Catalysis B: Environmental*, 200: 1–9.
29. Morgade, C. I. N. and Cabeza, G. F. (2017). First-principles study of codoping TiO_2 systems capable of improving the specific surface area and the dissociation of H_2O to generate H_2 and O_2. *Computational Materials Science*, 127: 204–210.
30. Zhang, R., Wang, Q., Liang, J., Li, Q., Dai, J. and Li, W. (2012). Optical properties of N and transition metal R (R=V, Cr, Mn, Fe, Co, Ni, Cu, and Zn) codoped anatase TiO_2. *Physica B: Condensed Matter*, 407(14): 2709–2715.
31. Gong, J., Yang, C., Zhang, J. and Pu, W. (2014). Origin of photocatalytic activity of W/N-codoped TiO_2: H_2 production and DFT calculation with GGA+U. *Applied Catalysis B: Environmental*, 152–153: 73–81.
32. Kumar, V. S. P. and Deshpande, P. A. (2019). Synergistic effect of metal-nonmetal substitution on oxygen activation in Pd/C- and Pd/N-substituted TiO_2. *Computational Materials Science*, 162: 349–358.
33. Perdew, J. P., Ruzsinszky, A., Csonka, G. I., Vydrov, O. A., Scuseria, G. E., Constantin, L. A., Zhou, X. and Burke, K. (2008). Restoring the density-gradient expansion for exchange in solids and surfaces. *Physical Review Letters*, 100(13): 136406.
34. He, Z., Yang, Q., Xi, G., Tu, J., Tian, J. and Zhang, L. (2023). Room-temperature ferroelectric-like behavior in anatase TiO_2 epitaxial films prepared by chemical solution deposition. *Applied Surface Science*, 625: 157193.
35. Lin, Y. M., Jiang, Z. Y., Hu, X. Y., Zhang, X. D., Fan, J., Miao, H. and Shang, Y. B. (2012). First-principles study of the electronic and optical properties of the (Y, N)-codoped anatase TiO_2 photocatalyst. *Chinese Physics B*, 21(3): 1–7.
36. Phillips, J. C. and Vechten, J. A. V. (1970). Spectroscopic analysis of cohesive energies and heats of formation of tetrahedrally coordinated semiconductors. *Physical Review B*, 2(6): 2147–2160.
37. Johari, N. A., Hamzah, N., Faizal, A. F. A., Samat, M. H., Hassan, O. H., Ali, A. M. M., Yahya, M. Z. A. and Taib, M. F. M. (2022). Effects of Hubbard U correction on the structural and electronic properties of rutile, anatase and brookite TiO_2. *Materials Today: Proceedings*, 66(P10): 4061–4067.
38. Zhao, Z., Zhao, X., Yi, J. and Liu, Q. (2015). Effects of nonmetal doping on electronic structures and optical property of anatase TiO_2 from first-principles calculations. *Rare Metal Materials and Engineering*, 44(7): 1568–1574.
39. Ye, H., Zuo, G. and Cao, Y. (2023). DFT computation of rare earth element doped TiO_2 anatase: Tunable absorption spectra for water splitting application. *Chemical Physics Letters*, 828: 140720.
40. Zeng, Z., Xu, M., Sun, Y., Xu, J. and Zhong, Y. (2022). First-principles study on the optical spectrum of N/P doped TiO_2-anatase. *Optik*, 261: 169231.
41. Liu, R., Yang, F., Xie, Y. and Yu, Y. (2019). Visible-light responsive boron and nitrogen codoped anatase TiO_2 with exposed {0 0 1} facet: Calculation and experiment. *Applied Surface Science*, 466: 568–577.
42. Rajput, P., Deshpande, M. P., Bhoi, H. R., Suchak, N. M., Desai, P. H., Chaki, S. H., Pandya, S. J., Mishra, M., Bhatt, S. V., Tiwari, D. K. and Sathe, V. (2022). Photocatalytic and antibacterial activity of Yttrium doped TiO_2 nanostructure. *Chemical Physics Impact*, 5: 100101.
43. Kushwaha, A. K., Khan, W., AlQahtani, H. R., Laref, A., Monir, M. E. A., Nya, F. T., Chowdhury, S., Alghamdi, E. A., Huang, H. M., Xiong, Y. C. and Yang, J. T. (2023). First-principles assessments of the electronic, and magneto-optical characteristics of Fe–Mn co-doped anatase TiO_2 for photo-catalysis applications. *Solid State Communications*, 360: 115059.
44. Jankov, S., Armaković, S., Tóth, E., Srdic, V., Cvejic, Z. and Skuban, S. (2020). Electronic structure of yttrium-doped zinc ferrite – Insights from experiment and theory. *Journal of Alloys and Compounds*, 842: 155704.
45. Jankov, S., Armaković, S., Tóth, E., Skuban, S., Srdic, V. and Cvejic, Z. (2019). Understanding how yttrium doping influences the properties of nickel ferrite – Combined experimental and computational study. *Ceramics International*, 45(16): 20290–20296.